

# The architecture of neoplastic follicles in follicular lymphoma; analysis of the relationship between the tumor and follicular helper T cells

William Townsend,<sup>1,2</sup> Marta Pasikowska,<sup>1</sup> Deborah Yallop,<sup>1,3</sup>  
Elizabeth H. Phillips,<sup>1</sup> Piers E.M. Patten,<sup>1,3</sup> Jonathan R. Salisbury,<sup>4</sup>  
Robert Marcus,<sup>3</sup> Andrea Pepper,<sup>5#</sup> and Stephen Devereux<sup>1,3#</sup>

<sup>1</sup>Department of Haematological Medicine, Rayne Institute, King's College London, London; <sup>2</sup>Department of Haematology, University College London Hospitals NHS Foundation Trust, London; <sup>3</sup>Department of Haematology, King's College Hospital, London; <sup>4</sup>Department of Histopathology, King's College Hospital, London and <sup>5</sup>Department of Clinical and Experimental Medicine, Brighton and Sussex Medical School, Brighton, UK

*#AP and SD are senior co-authors.*

©2020 Ferrata Storti Foundation. This is an open-access paper. doi:10.3324/haematol.2019.220160

Received: March 4, 2019.

Accepted: September 18, 2019.

Pre-published: September 19, 2019.

Correspondence: *WILLIAM TOWNSEND* - [william.townsend@nhs.net](mailto:william.townsend@nhs.net)

---

## Supplementary Material

### Preparation of slides for immunofluorescent confocal microscopy

FFPE LN blocks were cut into sections of 4 $\mu$ m or 12 $\mu$ m thickness, mounted onto Poly-L-Lysine coated slides and deparaffinized in xylene followed by rehydration in graded ethanol. Heat induced epitope retrieval was performed in pH 6.1 citrate buffer with 0.05% Tween 20 in a pressure cooker for 3 minutes. Sections were rehydrated before blocking in 5% normal donkey serum (Jackson ImmunoResearch, West Grove, Pennsylvania, USA) for 1 hour. Sections were then incubated with combinations of 3 or 4 primary antibodies with 0.025% Triton X-100 for 12 hours at 4°C in a humidified chamber. The antibodies used and their concentrations are listed in Table S3. The antibodies used in each combination were raised in different species to facilitate detection by species-specific secondary antibodies. After primary antibody incubation, slides were washed and then incubated with the appropriate combination of fluorescently-conjugated secondary antibodies and 4',6-diamidino-2-phenylindole dihydrochloride (DAPI) (Cell Signaling Technology, Danvers, USA) if a nuclear stain was required. Sections were mounted with coverslips using ProLong Gold Antifade mounting medium (Invitrogen, Carlsbad, California, USA).

Negative controls were run in parallel with all staining to ensure that the fluorescence detected was not due to non-specific binding of the secondary antibodies or tissue autofluorescence. Positive controls were reactive LNs or tonsil tissue. Additional controls were performed to ensure there was no spectral overlap of the fluorescently-conjugated antibodies.

### **Image acquisition**

All images were acquired on a Nikon Eclipse Ti-E upright microscope equipped with Nikon A1R Si confocal imaging system and lasers emitting at 405nm, 488nm, 561nm, and 642nm (Nikon Corporation, Tokyo, Japan). Low power images were obtained with a Pan Fluor x10 objective and high power images with a Pan Apo oil immersion x60 objective. To maintain consistency and to permit comparative analyses, all images were acquired on the same microscope and laser power, photo multiplier tube (PMT) gain, pixel dwell time, pin hole size, optical section thickness, offset, and filter settings were kept the same for analysis of paired control slides. These settings were maintained as closely as possible for all similarly stained sections but small differences in the thickness of tissue, quality of fixation, and the age of the specimen affected the strength of antibody binding, fluorescence and autofluorescence and accordingly, laser power, PMT gain, and offset were optimised for individual sections. 3-5 high power images (x60 objective) were obtained and analysed from representative follicular and interfollicular areas of each section.

### **Image analysis**

Binary layers were generated for each channel by setting thresholds to define which areas of an image were positive signal and included in the binary layer, and which areas were negative or background and excluded from the binary layer. Thresholding was performed on the basis of intensity of fluorescence in each channel and a size restriction to reduce false positive signal from small areas of autofluorescence. Large areas of autofluorescence or artefact from blood vessels or formalin crystals were deleted manually from the binary layers.

Generating binary layers for each channel permitted the accurate, automated quantification of the area of positive signal in an image, and the analysis of cellular co-localization. Areas

where combinations of antigens were expressed were calculated by defining 'intersecting' binary layers where the signal in 2 or more channels overlapped. This was used for example for identifying CD4<sup>pos</sup> cells that co-expressed PD-1 and ICOS; the proportion of CD4<sup>pos</sup> cells co-expressing these antigens was calculated by dividing the area of the CD4 PD-1 ICOS intersecting binary layer by the total area of the CD4 layer.

The proportion of proliferating cells in contact with T<sub>FH</sub> cells was calculated by defining individual cells in the Ki67 binary layer and automatically quantifying the proportion that were in direct contact with the intersecting binary layer of CD4 PD-1 or PD-1 ICOS (Figure S1).

For the analysis of CD20<sup>pos</sup> cells that were in contact with T<sub>FH</sub>, manual, visual analysis had to be performed as the diffuse pattern of CD20 staining and the closely packed nature of CD20<sup>pos</sup> cells meant that the automated analysis software was unable to reliably distinguish individual CD20<sup>pos</sup> cells that were not Ki67<sup>pos</sup>. To perform this, images were thresholded according to the method described above and binary layers of the intersecting CD3 and PD1 binary layers were created. A grid was superimposed over the image to aid visual assessment and to help ensure that each area of the image was inspected. A 'taxonomy tool' within the NIS elements software package was then used for the manual counting of Ki67<sup>pos</sup> and Ki67<sup>neg</sup> CD20<sup>pos</sup> B-cells that were, or were not in contact with T<sub>FH</sub>.

Due to the manual visual assessment of these images, two separate investigators analysed a subset of these images in order to identify and reduce operator bias. The two investigators were blinded to each other's results. There was no significant difference in number of Ki67<sup>pos</sup> cells counted by observer, the number of cells in contact with T<sub>FH</sub> was also concordant between operators.

Manual measurement was also used for analysis of BCL6 and FOXP3 images.

Images have been optimized for contrast using contrast settings and Look Up Tables (LUTs) and, where appropriate, magnification has been performed, no further image enhancement or manipulation has been used.

### **DNA extraction and TCR sequencing**

Equivalent areas of tissue were dissected from follicular and interfollicular areas. Genomic DNA was extracted using the miniDNA extraction kit (Qiagen, Venlo, Netherlands) according to the manufacturer's instructions.

### **TCR repertoire data analysis**

#### **Clonality index**

The clonality index was derived from Shannon's entropy, a measure of the certainty with which the identity of a clone selected randomly from a population of different clones can be predicted.<sup>(1)</sup> It is influenced by both the total number of different clones and the diversity of the population. Using this measure, a population or sample containing only one clone would have an entropy of 0, whilst a completely polyclonal population, in which all clones are equally frequent, would have a Shannon's entropy equal to the logarithm of the number of unique sequences. To allow populations containing different numbers of unique clones to be compared, the entropy was normalized by dividing by the logarithm of the number of unique clones present. The clonality index corresponds to the reciprocal of the normalized entropy so that a monoclonal population gives a value of 1 and a polyclonal population 0.

## Similarity index

The overlap between two populations was captured by the Jaccard index; the number of shared TCR sequences divided by the total number of distinct sequences in the two populations

## Statistical analysis

Statistical analysis was performed using GraphPad Prism software v5 (GraphPad Software Inc, La Jolla, California, USA). Normally distributed values are presented as the mean ( $\pm$  standard deviation), non-normally distributed values are presented as median ( $\pm$  interquartile range). Normally distributed variables were compared using two-tailed Students unpaired or paired t tests; non-normally distributed data were compared with Mann Whitney tests for unpaired and Wilcoxon paired rank test for paired data. Statistical significance was assumed when  $P$  was  $<0.05$ .

Contingency tables were used to determine whether  $Ki67^{pos}$  cells were more likely than  $Ki67^{neg}$  cells to be in contact with  $T_{FH}$ . Fisher's exact test was used to compare individual samples, for comparing total numbers of cells in multiple samples, Fisher's exact test was used for GCs, and Chi squared for FL.

For correlations e.g. between number of  $Ki67^{pos}$  cells and number of  $T_{FH}$ , Spearman non-parametric correlation coefficient was used.

**Supplementary tables**

Table S1: Clinical characteristics of FL patients

Sample	Age (years)	Gender	Grade	Stage	Disease status at biopsy	Prior therapy
FL001	68	Female	1	IV	relapse	R-CVP
FL002	88	Female	3b	I	untreated	not treated*
FL003	47	Male	2	IV	untreated	R-CVP
FL004	56	Male	2	IV	untreated	R-CHOP
FL005	45	Female	2	IV	untreated	R-CVP
FL006	41	Male	2	IV	untreated	R-CHOP + R
FL007	63	Female	3a	III	untreated	R-CHOP
FL008	60	Female	1	III	untreated	W&W
FL009	34	Female	3b	I	untreated	R-CHOP + RT
FL010	70	Female	2	III	relapse	R-CVP + R
FL011	58	Male	3b	III	untreated	R-CHOP
FL012	29	Male	2	IV	untreated	R-CVP
FL013	47	Female	1	IV	relapse	R-FC + ASCT
FL014	54	Male	2	III	untreated	W&W
FL015	57	Male	1	IV	untreated	R-CVP
FL016	32	Male	3a	IV	untreated	W&W
FL017	33	Male	1 - 2	IV	relapse	W&W
FL018	52	Male	1 - 2	IV	untreated	W&W
FL019	58	Male	3a	IV	relapse	R-bendamustine
FL020	38	Female	1 - 2	III	untreated	W&W
FL021	63	Female	1	III	untreated	W&W
FL022	88	Female	1	IV	relapse	R-CVP
FL023	62	Male	1 - 2	II	relapse	W&W
FL024	55	Female	3a	III	untreated	R-bendamustine
FL025	60	Male	3a	III	untreated	R-bendamustine

\* too frail to receive treatment and died due to ischemic heart disease and FL 5 months after diagnosis

R-CVP = rituximab, cyclophosphamide, vincristine, prednisolone. R-CHOP = rituximab, cyclophosphamide, doxorubicin, vincristine, prednisolone. W&W = watch and wait. RT = radiotherapy. R-FC = rituximab, fludarabine, cyclophosphamide. R = rituximab. CR = complete response. PR = partial response. HSCT = hematopoietic stem cell transplantation.

**Table S2: Clinical characteristics of patients with reactive lymph node biopsies**

<b>Sample</b>	<b>Age (years)</b>	<b>Gender</b>
rLN01	29	Male
rLN02	1	Male
rLN03	35	Female
rLN04	40	Female
rLN05	27	Male
rLN06	53	Female
rLN07	25	Male
rLN08	54	Female

**Table S3: Antibodies used for immunofluorescent labelling**

<b>Primary Antibodies</b>					
<b>Target</b>	<b>Species</b>	<b>Manufacturer</b>	<b>Clone</b>	<b>Dilution</b>	
CD3	Rat	Abcam	CD3-12	1:200	
ICOS	Rabbit	Abcam	SP98	1:100	
Ki67	Rabbit	Abcam	Polyclonal	1:100	
T-bet	Rabbit	Abcam	EPR9302	1:200	
CD8	Rabbit	Abcam	EP1150Y	1:400	
PD1	Goat	R&D systems	Polyclonal	1:50	
Ki67	Mouse	Leica Novocastra	MM1	1:100	
CD20cy	Mouse	Dako	L26	1:400	
Bcl-6	Mouse	Dako	PG-B6p	1:50	
CD4	Mouse	Leica Novocastra	4B12	1:50	
AID	Mouse	Invitrogen	ZA001	1:200	
PDL1	Rabbit	Spring Bioscience	SP142	1:200	
FOXP3	Mouse	Abcam	236A/E7	1:100	
<b>Species-specific Fluorescently conjugated Secondary Antibodies (all raised in Donkey)</b>					
<b>Target</b>	<b>Fluorochrome</b>	<b>Manufacturer</b>	<b>Dilution</b>	<b>Excitation Peak (nm)</b>	<b>Emission Peak (nm)</b>
Rat IgG	DyLight 405	Jackson	1:200	400	421
Rabbit IgG	DyLight 405	Jackson	1:200	400	421
Rabbit IgG	Alexa Fluor 488	Jackson	1:200	493	519
Rat IgG	Alexa Fluor 488	Jackson	1:200	493	519
Mouse IgG	Alexa Fluor 555	Life Technologies	1:200	555	565
Goat IgG	Alexa Fluor 647	Jackson	1:200	651	667
Rat IgG	Alexa Flour 647	Jackson	1:200	651	667

**Table S4. Number of unique TCR sequences in intra- and inter-follicular areas of FL LNs**

Case no	input DNA (ng)		No of unique TCRs		Unique TCRs/ng input DNA	
	F	IF	F	IF	F	IF
	P=0.05		P=0.06*		P=0.06	
FL01	218	402	1270	3450	5.83	8.58
FL02	336	764	1054	2044	3.14	2.68
FL03	341	376	822	2236	2.41	5.95
FL04	370	653	1901	7214	5.14	11.05
FL05	310	377	1033	2008	3.33	5.33

F= follicular region, IF = interfollicular region. TCRs = unique productive nucleotide reads of T-cell receptor CDR3 region. Significance of differences assessed by paired t test or Wilcoxon paired rank test\*.

**Supplemental Figure Legends:**

**Figure S1. Example of triple staining of a reactive lymph node showing how binary layers are created. Ai, Bi, and Ci** show each channel separately CD4 (red) ICOS (green), PD-1 (white). **Di** shows all channels together, CD4, ICOS, PD-1, and DAPI. **Aii, Bii, and Cii** show the binary layer for each channel. In **Dii** the binary layers for each channel are shown together. In **Diii** the area where CD4/PD1/ICOS intersection is shown in magenta highlighting the tight restriction of these CD4<sup>pos</sup>ICOS<sup>pos</sup>PD1<sup>pos</sup> cells to the germinal centre. Scale bars represent 50µm.

**Figure S2. Phenotype of intra- and interfollicular CD4<sup>pos</sup> T cells in FL (a)** Mean intensity of CD4 expression is significantly lower in the follicular CD4<sup>pos</sup> T-cells in FL than in interfollicular CD4<sup>pos</sup> T-cells (left) and the mean intensity of PD-1 in follicular CD4<sup>pos</sup>PD1<sup>pos</sup> T-cells is significantly higher than in interfollicular CD4<sup>pos</sup>PD1<sup>pos</sup> T-cells (right) (n= 81 follicular areas and 81 interfollicular areas from n=5 FL cases). **(b)** The intensity of expression of Bcl-6 is significantly higher in CD3<sup>pos</sup>PD-1<sup>pos</sup>ICOS<sup>pos</sup> cells than in PD-1<sup>neg</sup>ICOS<sup>neg</sup> T-cells but is highest in FL B-cells (n=290 cells from n=15 images in n=5 FL cases). Scale bar represents 5µm. **(c)** PD1<sup>pos</sup> ICOS<sup>pos</sup> cells within the follicles are CXCR5<sup>pos</sup> which further confirms their identity as T<sub>FH</sub> but is unhelpful in differentiating them from other follicularly located cells which all express CXCR5. **(d)** No CD8<sup>pos</sup> cells are found to express BCL6 confirming that CD3 is an acceptable surrogate for CD4 in these experiments.

**Figure S3. Distribution and phenotype of FOXP3<sup>pos</sup> cells in FL and GCs. (a1).** FOXP3<sup>pos</sup> cells are distributed mainly around the border of the follicle and there are also scattered FOXP3<sup>pos</sup> cells in the interfollicular areas (scale bar = 200 $\mu$ m). **(a2)** The area in the white rectangle in a1 has been enlarged. Some FOXP3<sup>pos</sup> cells express either ICOS or PD1 (scale bar = 50 $\mu$ m). **(b)** Binary layers of a high power (x60) image of a FL follicle are shown in each panel, **b1** some ICOS<sup>pos</sup> (green) cells are FOXP3<sup>pos</sup> (red). **b2** some PD1<sup>pos</sup> (blue) cells are FOXP3<sup>pos</sup>, but in **b3** few FOXP3<sup>pos</sup> cells are dually positive for both PD1 and ICOS. Overall, 25.0% (6.0-28.0) of ICOS<sup>pos</sup> and 4.0% (1.0-8.0) PD1<sup>pos</sup> T-cells expressed FOXP3, but only 5% (1.0-8.0) of dual positive ICOS<sup>pos</sup> PD1<sup>pos</sup> T-cells expressed FOXP3 (n= 12 images from n=3 FL samples). **(ci)** In reactive LNs, GCs FOXP3<sup>pos</sup> cells are located almost exclusively outside of the GCs. **(cii)** The same image as Ci showing only the binary layer of FOXP3 (red) highlighting the exclusion of FOXP3<sup>pos</sup> cells from the GCs.

**Figure S4. Ki67<sup>pos</sup> cells are CD20<sup>pos</sup> B-cells.** Representative low power (a) and magnified high power (b) images of 4 colour labelling in FL showing that 96% of Ki67<sup>pos</sup> cells are CD20<sup>pos</sup> B-cells. CD20 (red), Ki67 (blue), PD-1 (white), CD3 (green). Scale bars, **a** = 100 $\mu$ m, **b** = 10 $\mu$ m.

**Figure S5. AID positive Ki67 cells are in close contact with PD-1<sup>Hi</sup> cells. (A1)** Representative image showing Ki67<sup>pos</sup> (green) AID<sup>pos</sup> (red) cells in close contact with PD-1<sup>Hi</sup> (white) cells, scale bar represents 25 $\mu$ m. **(A2)** Magnified area of **1** highlighting close association between AID<sup>pos</sup> Ki67<sup>pos</sup> cells and PD-1<sup>Hi</sup> cells, scale bar represents 5 $\mu$ m. Images representative of n=16 images from n=6 samples. **(b)** Negative control demonstrating that signal seen in red channel is not autofluorescence or false positive signal from secondary antibody (negative control performed by labelling with the same secondary antibodies as in figure S5a but with no primary antibodies, counterstained with DAPI, image obtained using same laser power

settings and LUTs as S5a. (c) Representative z-stack image showing similar intra-cellular pattern of AID staining (red) in reactive GCs, and close localization of AID<sup>pos</sup> Ki67<sup>pos</sup> cells with PD1<sup>pos</sup> cells in the light zone.

**Figure S6. PD-L1 is not present on the Ki67<sup>pos</sup> cells in contact with PD1<sup>Hi</sup> cells.** Representative low power (a) and high power (b) images of FL showing that PD-L1 (green) is not highly expressed on the Ki67<sup>pos</sup> cells (red) that are in contact with PD-1<sup>Hi</sup> cells (white). Scale bars represent 100 $\mu$ m (a) and 25  $\mu$ m (b). (c) PD-L1 is mainly found outside of the follicles and is not present on CD23<sup>pos</sup> follicular dendritic cells (PD-L1, green. CD23, white. CD20, red). Scale bar represents 100 $\mu$ m.

In each case, the more frequent clones predominate in the follicular regions compared to the interfollicular areas

Figure S7. **Association between area of Ki67 and T<sub>FH</sub> in reactive GCs.**  $r = 0.55$ ,  $P = 0.019$ ,  $n=17$  GCs from  $n=4$  samples

**Figure S8: Proportion of CD4<sup>pos</sup> cells with dual expression of PD1 and ICOS by histological grade in FL.** There is no significant difference in the proportion of CD4<sup>pos</sup> T cells that have a T<sub>FH</sub> phenotype by histological grade in FL,  $p = 0.21$ .

## Supplemental Figures:

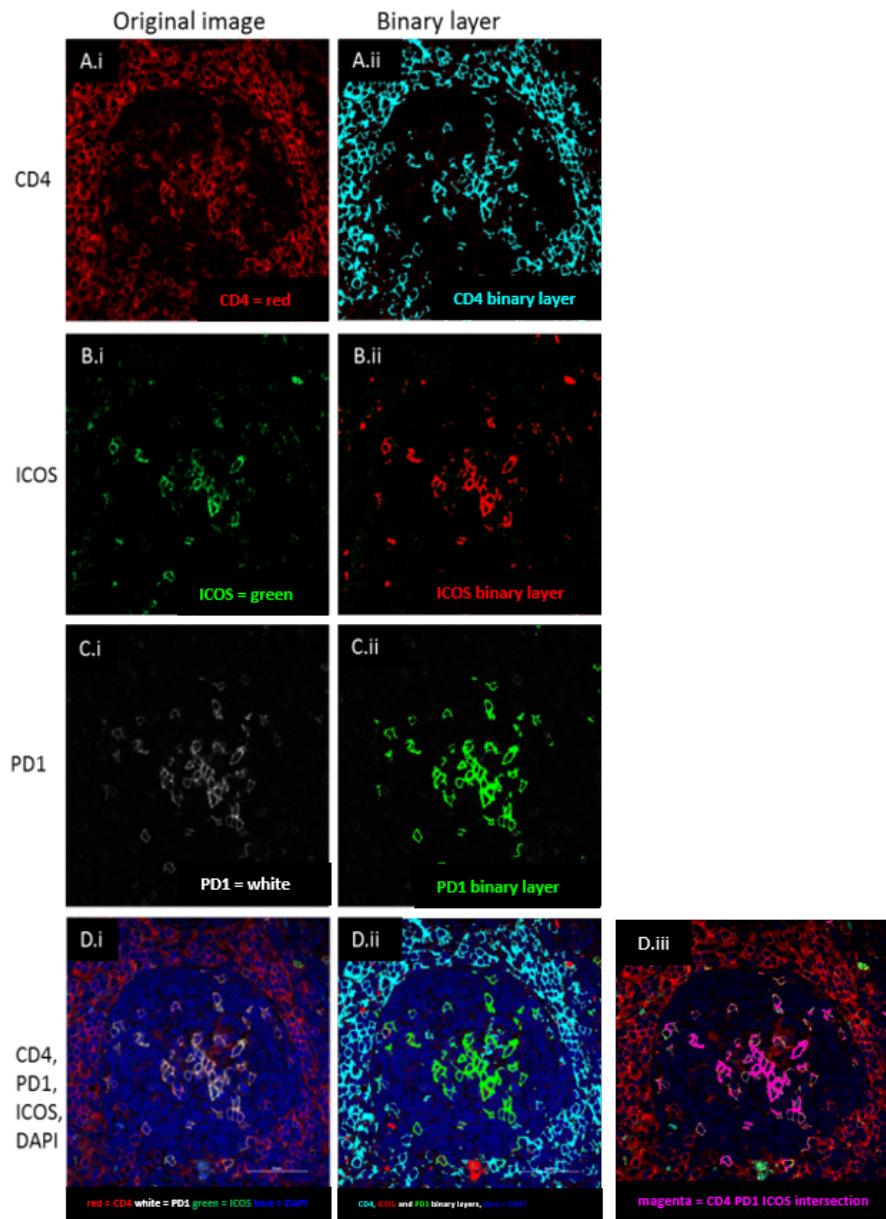


Figure S1

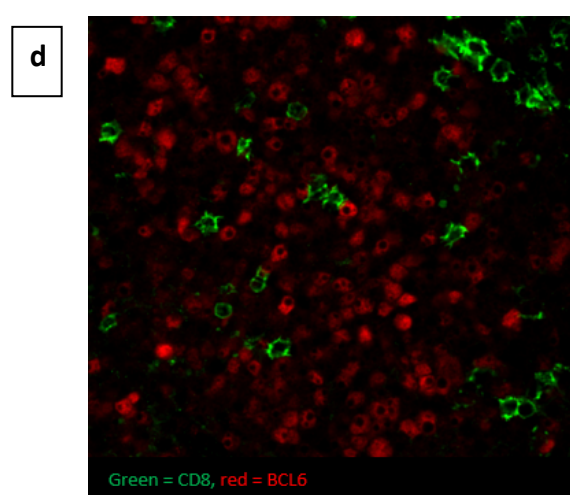
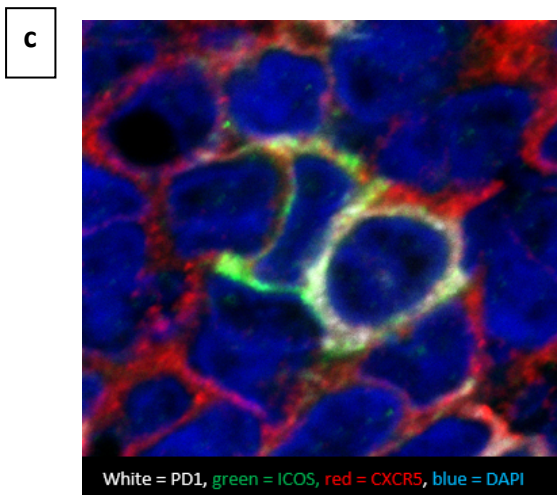
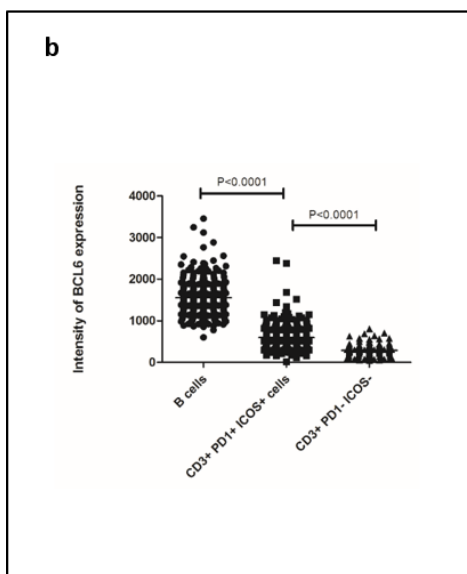
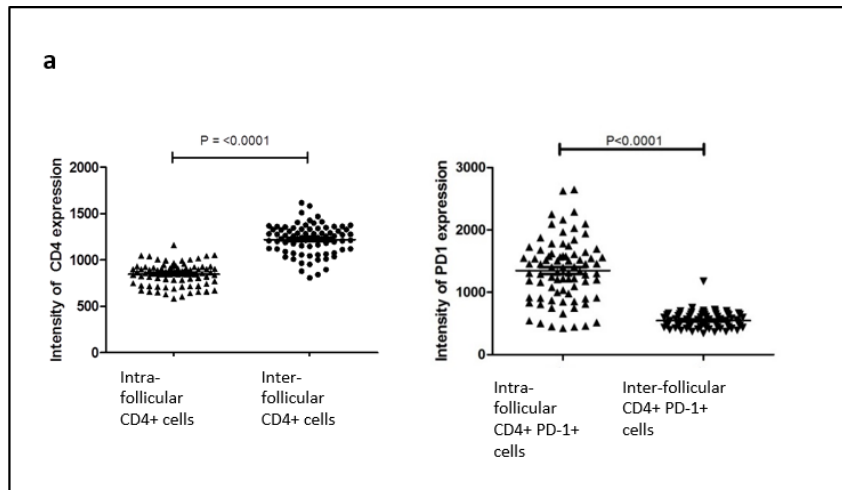


Figure S2

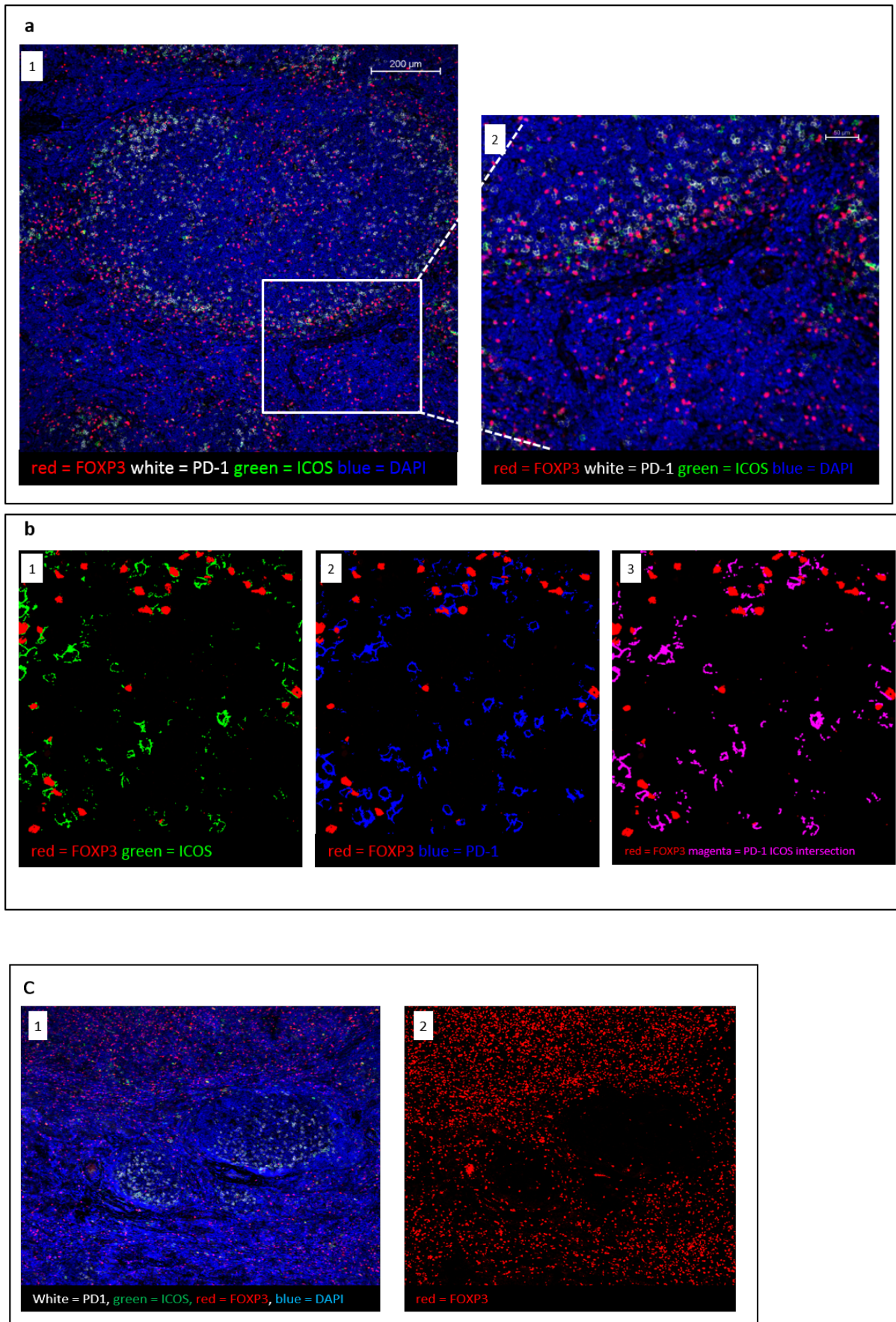


Figure S3

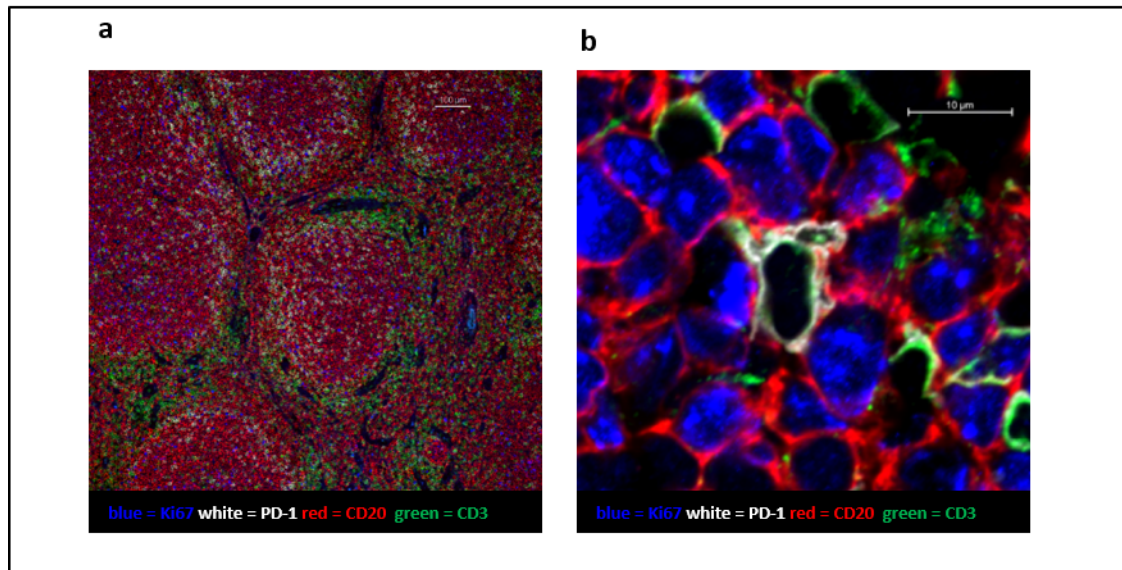
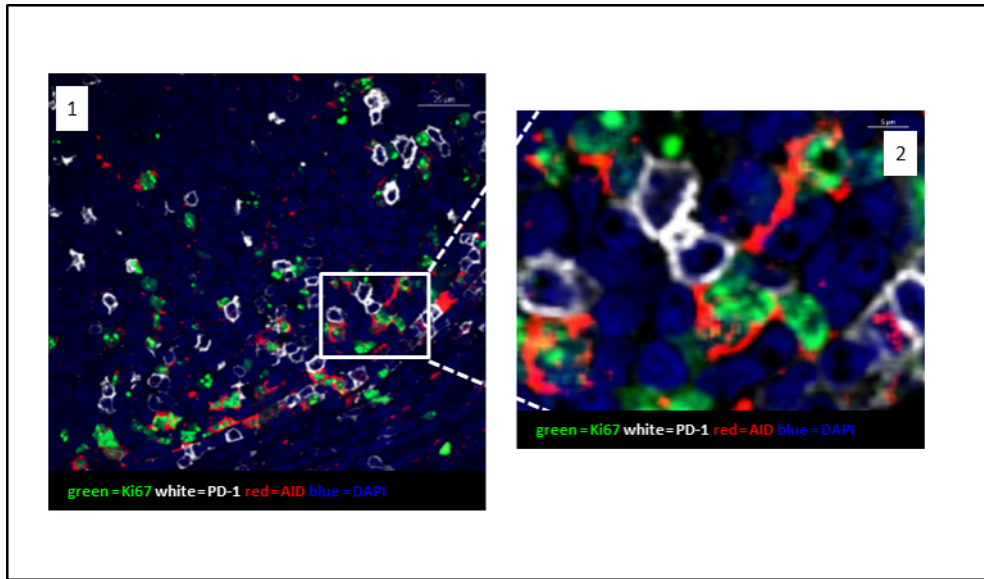
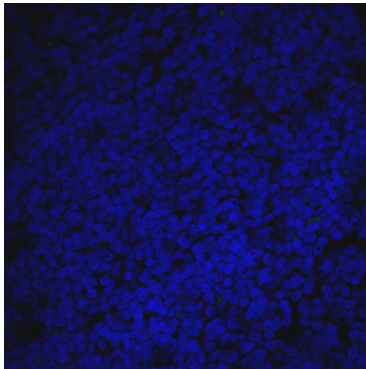


Figure S4

a



b



c

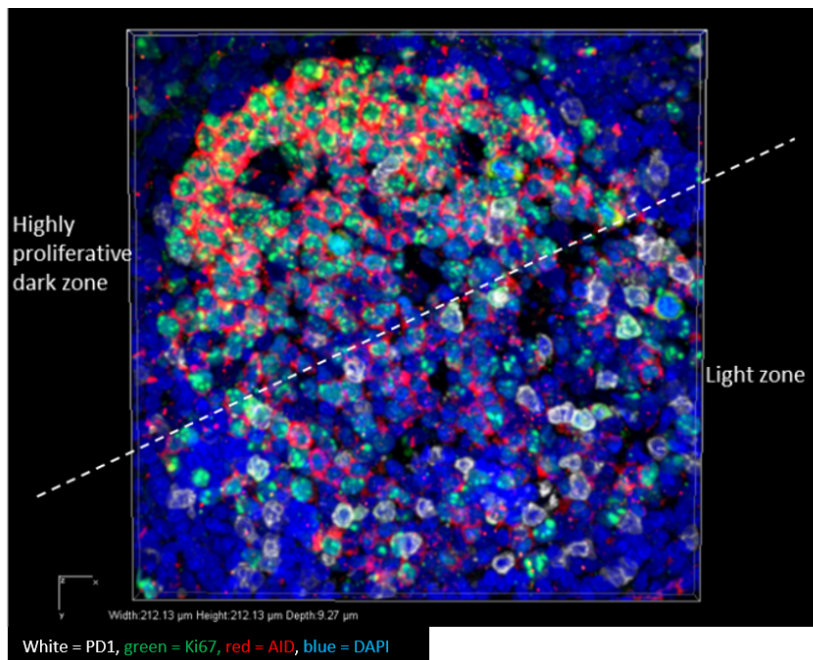


Figure S5

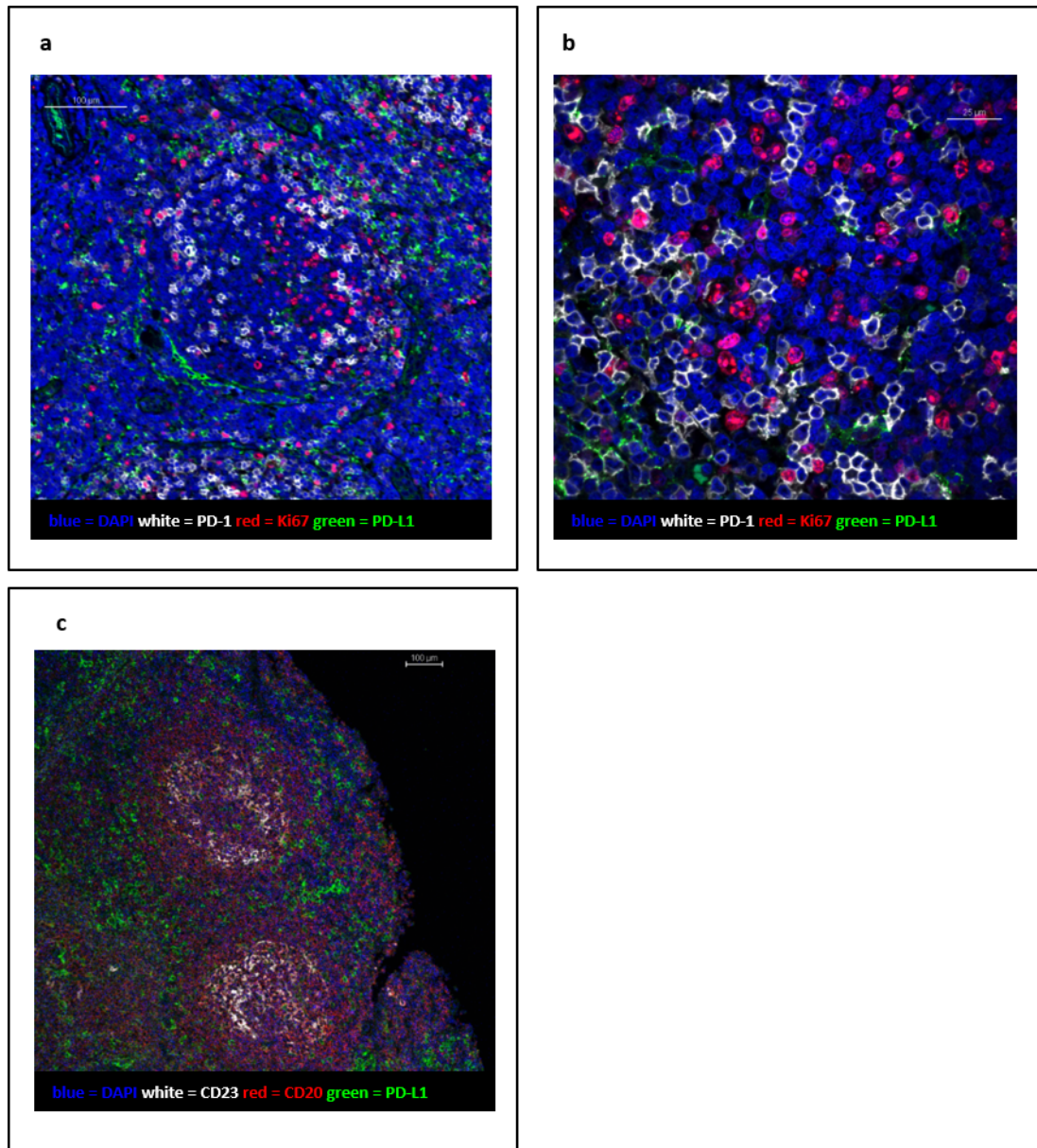
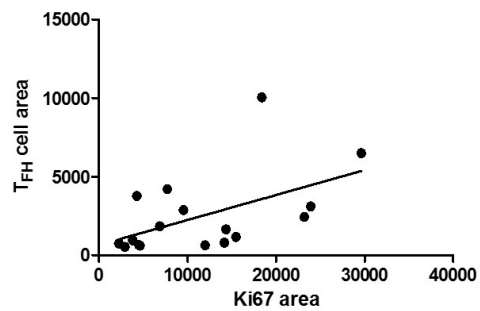
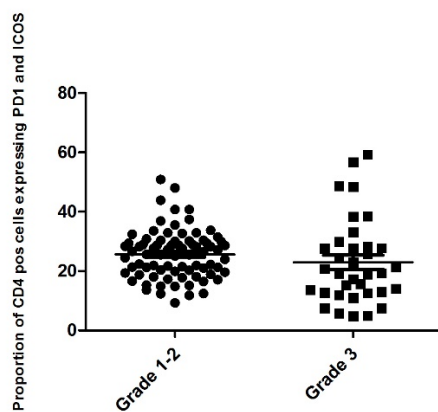


Figure S6

**Figure S7****Figure S8**

## References

1. Sherwood AM, Emerson RO, Scherer D, et al. Tumor-infiltrating lymphocytes in colorectal tumors display a diversity of T cell receptor sequences that differ from the T cells in adjacent mucosal tissue. *Cancer Immunol Immunother.* 2013;62(9):1453-1461.